American Mineralogist, Volume 66, pages 1135–1153, 1981

Devolatilization equilibria in H_2O–CO_2 and H_2O–CO_2–NaCl fluids: an experimental and thermodynamic evaluation at elevated pressures and temperatures

G. K. JACOBS[1] AND D. M. KERRICK

Department of Geosciences
The Pennsylvania State University
University Park, Pennsylvania 16802

Abstract

Experimental equilibrium brackets have been obtained in H_2O–CO_2 and H_2O–CO_2–NaCl fluids for several decarbonation equilibria. Using available thermodynamic data and activities for H_2O and CO_2 calculated from the modified hard-sphere Redlich-Kwong (HSMRK) equation of Kerrick and Jacobs (1981), thermodynamic extrapolations in P–T–X_{CO_2} space of devolatilization equilibria yield close agreement with the experimental equilibrium brackets, implying that the experimental and thermodynamic data are internally consistent, and that the activities of H_2O and CO_2 predicted by the HSMRK equation of Kerrick and Jacobs (1981) are quite reasonable. The significance of assuming ideal vs. non-ideal mixing of H_2O and CO_2 for the calculation of T–X_{CO_2} topologies is demonstrated for a portion of the system CaO–Al_2O_3–SiO_2–H_2O-CO_2. Experiments in H_2O–CO_2–NaCl mixtures at P = 6 kbar show that, compared to binary H_2O–CO_2 fluids, the presence of small (5–10 wt.%) amounts of NaCl in the fluid phase significantly increase the activity of CO_2 for H_2O-rich compositions. At 2 kbar, however, little difference in the activity of CO_2 in H_2O–CO_2–NaCl vs. H_2O–CO_2 mixtures is implied by the experiments.

Introduction

Many authors (*e.g.*, Chernosky, 1979; Kerrick and Ghent, 1979; Kerrick and Slaughter, 1976; Perkins *et al.*, 1977, 1980; Slaughter *et al.*, 1975) have pointed out that direct experimentation as the only means of determining P–T–X_{CO_2} topologies for metamorphic systems is not practical. The time required to experimentally determine the P–T–X_{CO_2} coordinates of all important metamorphic equilibria over a wide range of pressure and temperature is prohibitive. Moreover, some equilibria (*e.g.*, those stable at very low P–T conditions) may not be amenable to direct experimentation. Therefore, as the above authors conclude, the combination of careful experimentation and thermodynamic extrapolations is the best practical approach.

Helgeson *et al.* (1978), Kerrick and Ghent (1979), Kerrick and Slaughter (1976), Perkins *et al.* (1977, 1980), Slaughter *et al.* (1975), and Wall and Essene (1972) have shown that thermodynamic P–T extrapolations for many solid–solid and dehydration ($P_{H_2O} = P_{total}$) equilibria are in close agreement with experimental determinations of the equilibria over a wide P–T range. This agreement implies that the available thermodynamic data for the solids and H_2O are consistent with the independently derived experimental equilibrium brackets. Helgeson *et al.* (1978), in deriving an internally consistent set of enthalpies and free energies of formation for minerals through the combination of experimental phase equilibrium data and thermodynamic calculations, used decarbonation and mixed-volatile equilibria only when no other choice was available. According to Helgeson *et al.* (1978), this was because of a lack of reliable fugacities for CO_2 (particularly at $P \geq 5$ kbar) and the lack of a reliable method for predicting activities in H_2O–CO_2 mixtures at elevated pressures and temperatures. Shmulovich and Shmonov (1978) have since provided fugacities for CO_2 to 1000°C and 10 kbar which are in good agreement with the unpublished data of Burnham and Wall. In comparing mixed-volatile equilibria calculated from thermochemical data *versus* that obtained experimentally, Helgeson *et al.* (1978)

[1]Present address: Rockwell Hanford Operations, P.O. Box 800, Richland, Washington 99352.

0003–004X/81/1112–1135$02.00

found that Holloway's (1977) adaption of the MRK equation for H_2O–CO_2 mixtures yielded inconsistent agreement; however, Flower's (1979) subsequent correction of Holloway's (1977) formulation improved this correlation.

Because much of the experimental data on activities in H_2O–CO_2 mixtures has been obtained over very restricted P–T ranges (*e.g.*, Chou and Williams, 1977, 1979a, 1979b; Eggler and Burnham, 1978; Eggler and Kadik, 1979; Eggler *et al.*, 1979, Franck and Tödheide, 1959; Gehrig *et al.*, 1979; Greenwood, 1969, 1973; Jacobs and Kerrick, 1979; Shmulovich, 1977; Walter, 1963; Ziegenbein and Johannes, 1980), an equation of state which predicts accurate activities in H_2O–CO_2 mixtures over a wide range of pressure and temperature would be useful for accurately calculating P–T–X_{CO_2} topologies. Kerrick and Jacobs (1981) derived a hard-sphere modified Redlich-Kwong (HSMRK) equation of state for H_2O and CO_2 which predicts mixing properties of H_2O and CO_2 that are in good agreement with much of the available experimental data on H_2O–CO_2 mixtures. The analysis of Kerrick and Jacobs (1981) also suggests that the HSMRK equation is superior to Holloway's (1977) MRK equation (corrected version of Flowers, 1979) for prediction of the thermodynamic properties of H_2O, CO_2 and their mixtures to pressures and temperatures above the P–T range of the available P–V–T data.

Comparisons between calculated and experimentally determined devolatilization equilibria in P–T–X_{CO_2} space provide a test for the available thermodynamic data of pure solids, pure gases (H_2O and CO_2), and the activities of H_2O and CO_2 in H_2O–CO_2 mixtures predicted by the HSMRK equation. Experimental determinations of the P–T–X_{CO_2} conditions of equilibria invlving *both* H_2O and CO_2 as components allow an evaluation of the product or ratio (as dictated by the equilibrium constant) of the activity coefficients of H_2O and CO_2. However, experimental determinations of dehydration and decarbonation equilibria allow a direct evaluation of the activity coefficients for H_2O and CO_2, respectively, not just a ratio or product. Unfortunately, most dehydration equilibria are not stable over a wide range of X_{CO_2}, making them unsuitable for such an analysis. Therefore, in addition to an analysis of previously published experimental work, the following decarbonation equilibria, stable over a wide range of fluid compositions, were studied experimentally in H_2O–CO_2 mixtures:

$$\text{calcite} + \text{quartz} = \text{wollastonite} + CO_2 \quad (1)$$

$$\text{dolomite} + 2\ \text{quartz} = \text{diopside} + 2\ CO_2 \quad (2)$$

$$\text{calcite} + \text{quartz} + \text{andalusite} = \text{anorthite} + CO_2 \quad (3a)$$

$$\text{calcite} + \text{quartz} + \text{kyanite} = \text{anorthite} + CO_2 \quad (3k)$$

$$\text{calcite} + \text{quartz} + \text{rutile} = \text{sphene} + CO_2 \quad (4)$$

In order for calculated P–T–X_{CO_2} topologies to better represent geologic systems, the presence of components in addition to H_2O and CO_2 in the fluid phase must be considered. Jacobs and Kerrick (1981a) have considered the effect of the presence of small amounts of CH_4 on activities in H_2O–CO_2–CH_4 mixtures, and the resulting effect on P–T–X_{CO_2} topologies of metamorphic systems. In addition to CH_4, chloride species have been shown to be present in significant amounts in geologic fluids (*e.g.*, Crawford *et al.*, 1979a,b; Hendel and Hollister, 1981; Hollister and Burruss, 1976; Hollister *et al.*, 1979; Konnerup-Madsen *et al.*, 1979; Luchscheiter and Morteani, 1980; Pêcher, 1979; Rich, 1979; Roedder, 1972). Expansion of the H_2O–CO_2 solvus resulting from the addition of NaCl (Gehrig *et al.*, 1979; Hendel and Hollister (1981); Hollister and Burruss, 1976; Takenouchi and Kennedy, 1965) may imply an increase in the activity of CO_2 and/or H_2O relative to the activities in binary H_2O–CO_2 mixtures. This increased activity may have a significant effect on the stability of mineral assemblages in equilibrium with H_2O–CO_2–NaCl fluids relative to assemblages in equilibrium with binary H_2O–CO_2 mixtures. Because the T–X_{CO_2} position of a devolatilization equilibrium is dependent upon the activity of H_2O and/or CO_2 (in addition to the thermodynamic properties of the solid phases involved), a representative devolatilization equilibrium was chosen to experimentally compare equilibrium determinations in H_2O–CO_2 mixtures to results in H_2O–CO_2–NaCl mixtures.

Experimental techniques

The techniques discussed below are similar to those used by Eggert and Kerrick (1981), Hunt and Kerrick (1977), Kerrick and Ghent (1979), and Slaughter *et al.* (1975).

In the experiments, quartz was taken from a large single crystal of clear Brazilian quartz. Table 1 contains the sample provenance, a chemical analysis, and a structural formula for other minerals used

Table 1. Chemical composition of starting materials

	Rutile[a] (Alexander Co., North Carolina)	Sphene[a] (Capelinha, Minas Gerais, Brazil)	Anorthite[b] (Miyake Is., Honshu, Japan)	Wollastonite[b] (Willsboro, New York)	Andalusite[b] (Minas Gerais, Brazil)	Kyanite[b] (North Carolina)	Calcite[c]	Dolomite[d]	Diopside[d]
SiO_2	-	30.49	43.97	50.93	37.10	36.90	0.001	<0.10	54.50
TiO_2	99.91	38.11	-	-	-	<0.02	<0.001	<0.02	<0.02
Al_2O_3	-	0.91	35.61	<0.01	62.10	62.80	<0.001	-	<0.05
Fe_2O_3	-	0.63	-	0.02	0.38	0.13	-	0.79	-
FeO	0.54	-	0.39	-	-	-	<0.001	-	0.61
MnO	-	-	<0.01	0.01	0.04	<0.02	-	0.08	0.06
MgO	-	-	-	-	-	<0.02	<0.001	21.19	18.00
CaO	-	28.44	19.93	48.77	-	-	56.03	30.99	25.60
Na_2O	-	-	0.45	0.02	-	-	-	<0.05	<0.05
SrO	-	-	-	-	-	-	-	<0.025	-
H_2O	-	0.28	-	-	-	-	0.001	-	-
CO_2	-	-	-	-	-	-	43.97	46.90	-
F	-	0.20	-	-	-	-	-	-	-
Total	100.45	99.06	100.36	99.75	99.62	99.89	100.006	99.95	98.77

Structural Formulas:

Rutile: $Ti_{0.997}Fe_{0.006}O_2$

Sphene: $Ca_{1.00}(Ti_{0.94}Fe_{0.02}Al_{0.04})\ Si_{1.00}(OH_{0.06}\ F_{0.02}\ O_{4.92})$

Anorthite: $(Ca_{0.988}Na_{0.04})(Al_{1.941}Fe_{0.02}Mn_{0.02})\ Si_{2.032}O_8$

Wollastonite: $Ca_{1.017}Na_{0.01}Si_{0.991}O_3$

Andalusite: $(Al_{1.986}Fe_{0.009}Mn_{0.002})\ Si_{1.006}O_5$

Kyanite: $(Al_{2.001}Fe_{0.003})\ Si_{0.997}O_5$

Calcite: $Ca_{1.00}(CO_3)_{1.00}$

Diopside: $Ca_{1.00}(Mg_{0.98}Fe_{0.02})\ Si_{2.00}O_{6.00}$

Dolomite: $Ca_{1.03}(Mg_{0.98}Fe_{0.02})(CO_3)_{1.98}$

[a]Analysis from Hunt and Kerrick (1977).

[b]Analysis from Kerrick and Ghent (1979).

[c]Analysis from Eggert and Kerrick (1981).

[d]Analysis from Slaughter et al. (1975).

in this study. Each sample was crushed to less than 325 mesh and elutriated in distilled water to remove the ultrafine particles.

Starting mixtures for equilibrium 1 consisted of calcite + quartz (equal weights) and wollastonite loaded into separate Ag_{50}–Pd_{50} capsules. For equilibria 2–4, however, starting mixtures consisted of equal weights of each solid reactant and product, with a quartz sphere replacing powdered quartz in one set of experiments for equilibrium 3k.

H_2O–CO_2 fluids were generated by adding known amounts of H_2O and silver oxalate ($Ag_2C_2O_4$) to capsules containing approximately 0.03 g of a starting mixture. The solid to fluid ratio was maintained at a constant value of approximately 5 to 1 (by weight). Compositions at the end of a run were

determined by the weight loss method of Johannes (1969). Analysis of "blank" capsules (initially containing only H_2O and silver oxalate) indicated that the error in determining X_{CO_2} was probably less than ±0.01. Aqueous solutions of 5 and 10 wt.% NaCl (0.90 and 1.90 molal, respectively), along with silver oxalate, were used to generate the fluid phase for runs with H_2O–CO_2–NaCl mixtures.

Runs at 2 and 6 kbar were respectively performed in cold-seal pressure vessels (H_2O pressure medium) and internally-heated pressure vessels (Ar pressure medium). The cold-seal pressure vessels were mounted horizontally and contained filler rods to minimize temperature measurement error (Boettcher and Kerrick, 1971). Pressures were monitored with bourdon-tube gauges (estimated error = ±50 bars) for the cold-seal vessels, while a manganin cell (estimated error = ±1%) was used for the internally-heated vessels. Temperatures (±7°C) in the cold-seal vessels were measured with external, inconel-sheathed, chromel-alumel thermocouples. Temperatures (±5°C) in the internally-heated vessels were measured with three internal, inconel sheathed, chromel-alumel thermocouples. Based on extensive testing of other thermocouples of this type against reference thermocouples constructed of wire calibrated by the National Bureau of Standards, the accuracy of the sheathed thermocouples is estimated to be ±2–3°C. The stated errors in the run temperatures include temperature fluctuation and an estimate of the error in accuracy. Quench duration was approximately three and five minutes for the cold-seal and internally-heated vessels, respectively. In all cases run duration was 7 days.

For equilibria (2–4), reaction direction was determined by monitoring the mass of CO_2 lost or gained during a run. Since the decarbonation reactions studied involved CO_2 as the only gas component, the difference between the final and initial number of moles of CO_2 is a direct measure of reaction direction. Uncertainty associated with the value of Δmoles CO_2 (final moles minus initial moles) is believed to be less than $\pm 1 \times 10^{-6}$ moles. Isothermal–isobaric runs were conducted for multiple capsules with a series of different initial X_{CO_2} values. As a check on experimental equilibrium data obtained by monitoring compositional changes of the fluid, reaction 3k was also monitored by the weight change of quartz spheres.

Equilibrium 1 was not amenable to monitoring changes in the mass of CO_2, since, as Jacobs and Kerrick (1980) have shown, the quench reaction: wollastonite + CO_2 → calcite + SiO_2 (aq.) is very rapid. This reaction results in anomalous changes in the mass of CO_2 gained or lost during a run, thus complicating interpretation of the results. Therefore, calcite + quartz and wollastonite were loaded into separate capsules and run isothermally–isobarically at a series of initial X_{CO_2} values. Reaction direction was measured by Gunier X-ray detection (minimum detectability = 1–2% by volume) of spontaneous nucleation and growth of new phases.

Experimental results

Table 2 contains the experimental equilibrium brackets for all equilibria studied. Results for individual equilibria in both H_2O–CO_2 and H_2O–CO_2–NaCl fluids are discussed below.

H_2O–CO_2 fluids

Table 3 summarizes the experimental results on equilibrium 1. Because the starting mixture in runs 1–6 was calcite + quartz, runs in the stability field of wollastonite should evolve CO_2 (thereby increasing X_{CO_2}), whereas runs in the stability field of calcite + quartz should show no change in X_{CO_2}. Because of back reaction during the quench, the

Table 2. Summary of experimental equilibrium brackets

Equilibrium No.	P(kb)	T(°C)	X_{CO_2}	wt.% NaCl
(1)	6	880	0.86 ± 0.03	0.0
(2)	5	575	0.60 0.02	0.0
(3a)	2	370	0.13 0.04	0.0
	2	400	0.27 0.07	0.0
	2	450	0.69 0.03	0.0
(3k)	6	460	0.05 0.02	0.0
	6	500	0.17 0.03	0.0
	6	575	0.75 0.03	0.0
(4)	2	420	0.15 0.05	0.0
	2	450	0.30 0.05	0.0
	2	500	0.57 0.05	0.0
	2	520	0.78 0.03	0.0
(4)	6	500	0.09 0.02	0.0
	6	550	0.25 0.02	0.0
	6	575	0.48 0.02	0.0
	6	600	0.65 0.02	0.0
	6	620	0.82 0.03	0.0
(4)	2	450	0.20 0.03	5.0
	2	475	0.52 0.04	5.0
	2	520	0.67 0.02	5.0
(4)	2	450	0.18 0.03	10.0
	2	475	0.53 0.04	10.0
	2	520	0.68 0.02	10.0
(4)	6	550	0.18 0.02	5.0
	6	575	0.25 0.03	5.0
	6	600	0.70 0.02	5.0
(4)	6	550	0.17 0.02	10.0
	6	575	0.19 0.02	10.0
	6	600	0.68 0.02	10.0

Table 3. Run data for the reaction: calcite + quartz ⇄ wollastonite + CO_2 at P = 6 kbar, T = 880°C

Run No.	Starting material	Products	Initial* X_{CO_2}	Final* X_{CO_2}	Reaction direction
1	cc+qtz	cc+qtz+wo	0.500	0.617	→ wo
2	cc+qtz	cc+qtz+wo	0.655	0.768	→ wo
3	cc+qtz	cc+qtz+wo	0.715	0.786	→ wo
4	cc+qtz	cc+qtz+wo	0.806	0.842	→ wo
5	cc+qtz	cc+qtz	0.885	0.885	—
6	cc+qtz	cc+qtz	0.980	0.980	—
11	wo	wo	0.885	0.885	—
12	wo	wo+cc+qtz	0.980	0.895	cc+qtz ←

*The precision error in measurements of X_{CO_2} is ± 0.01.

X_{CO_2} value of run 4 (see Table 3) represents the *minimum* X_{CO_2} value of the equilibrium bracket, since runs 5 and 6 showed no apparent reaction. Run 12 (see Table 3), with nucleation and growth of calcite + quartz (detected by X-ray diffraction), defines the maximum value of X_{CO_2} for equilibrium 1 because run 11, at a slightly lower X_{CO_2} value, had no apparent reaction. There should be no complications involving reaction during the quench for runs 11 and 12, because quench reactions involving wollastonite in H_2O–CO_2 fluids are minimized at high values of X_{CO_2} (Jacobs and Kerrick, 1980).

Results of the experiments on equilibria 2–4 in H_2O–CO_2 mixtures are summarized in Figures 1–5. For each set of runs, the change in the number of moles of CO_2 during a run is plotted against the final X_{CO_2} value. In Figure 3 (500°C run), the change in moles of quartz is plotted in addition to change in moles of CO_2. The weight of quartz spheres before and after the run (an average of 5 replicate weighings; see Hunt and Kerrick, 1977) defined the change in moles of quartz. As expected from the stoichiometry of equilibrium (3k), the change in moles of quartz is approximately symmetrical with the CO_2 data. Optical and X-ray analysis of run products indicated that no unwanted phases nucleated during the runs represented in Figures 1–5. In addition, because decarbonation equilibria were studied, the constant mass of H_2O before and after the runs suggests that no competing reactions involving H_2O occurred.

A second degree polynomial (Δmoles = $f(X_{CO_2})$) was fit to each set of data using the least-squares regression program 'Minitab 2' (Ryan *et al.*, 1976).

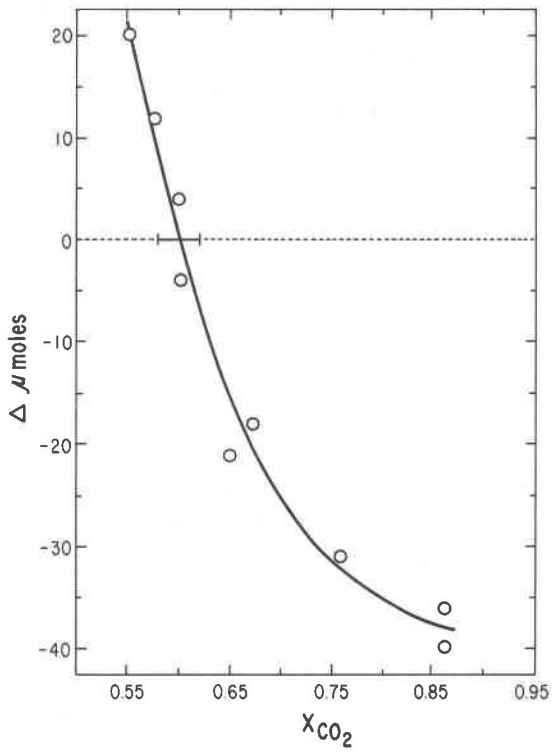

Fig. 1. Experimental data pertaining to equilibrium 2 in H_2O–CO_2 mixtures at P = 5 kbar, T = 575°C. This is a plot of $\Delta\mu$moles of CO_2 as a function of final fluid composition. The curve was fit by least squares to the experimental data. The bracket at $\Delta\mu$moles = 0 represents the intersection of a $\pm 2\sigma$ band about the regression curve and the line of zero change.

The form of the equation, fit to all the data of this study, was arbitrarily chosen, since a theoretically valid equation which fits the data is not known at this time. The X_{CO_2} value where a curve passes through the line of Δmoles = 0 is taken to represent

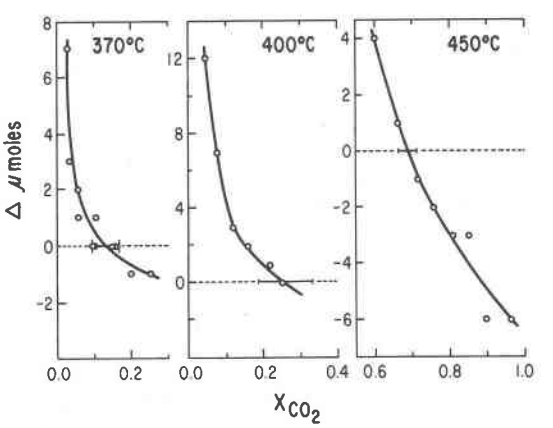

Fig. 2. Experimental data pertaining to equilibrium 3a in H_2O–CO_2 mixtures at P = 2 kbar. Significance of the curves and brackets is identical to those in Figure 1.

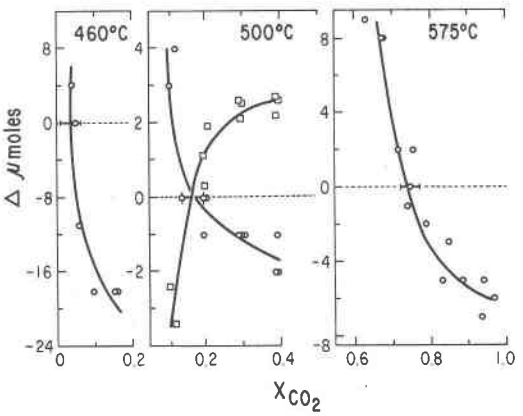

Fig 3. Experimental data pertaining to equilibrium 3k in H_2O–CO_2 mixtures at P = 6 kbar. This is a plot of $\Delta\mu$moles of CO_2 (circles) and Δmoles of quartz (squares) as a function of final fluid composition. Significance of the curves and brackets is identical to those in Figure 1.

the equilibrium X_{CO_2} value at the pressure and temperature of each experiment. The width of a given bracket (see Figs. 1–5) is defined by the intersection of a $\pm 2\sigma$ band about the regression curve and the line of Δmoles = 0.

This method of determining equilibrium is identical to that of Eggert and Kerrick (1981). It represents a refinement in the method of equilibrium determination in earlier studies in our laboratory by Slaughter *et al.* (1976), and Hunt and Kerrick (1977), which utilized experimental techniques and data analysis similar to that of Eggert and Kerrick (1981) and the present paper. In much of the present study, reaction direction in each run was monitored by the number of moles of CO_2 consumed or formed. Accordingly, as in experiments monitoring the weight change of a single crystal of a reaction component, these experiments provide a monitor of the reaction rate. In each set of runs leading to an equilibrium bracket, P, T, run duration, and grain size were held constant. Thus, the changes in moles of CO_2 recorded in Figures 1–5 are a function of the initial X_{CO_2} in the charge. As confirmed by these diagrams, smaller changes in the moles of CO_2 will occur for runs with initial X_{CO_2} values close to the equilibrium value. For a given reaction on an isobaric, isothermal plot of Δmoles CO_2 *vs.* X_{CO_2}, curves for different combinations of run duration and fluid/solid ratios will have different slopes but will share the same intercept at the equilibrium X_{CO_2} value. The scatter of the data points about each of the curves plotted in Figures 1–5 reflects precision uncertainty. Least squares fits to the data points neglect the precision uncertainty in each of the data points. The validity of the curve-fitting technique is enhanced by the fact that error distribution about each data point is "normal" (Gaussian) rather than "rectangular". Thus, within the error envelope of each data point, the midpoint represents the most probable value. Accordingly, uncertainties in our data points fit the basic requirements for curve-fitting by the least-squares method (Daniel and Wood, 1971). As is standard with this technique, error in the fitted curve is assigned to the dependent variable; thus, uncertainty in the fitted curves in Figures 1–5 corresponds to an error band of $\pm 2\sigma$ in Δmoles CO_2. As illustrated by Eggert and Kerrick (1981), this method of determining equilibrium brackets avoids ambiguities that can appear using the "classical" bracketing technique. An excellent example of such problems is illustrated in Figure 1. Because of the scatter of data points at $X_{CO_2} = 0.60$, the usual approach would be to select the next nearest set of meaningful bracketing points—in this case, the lower bracketing point would be that at

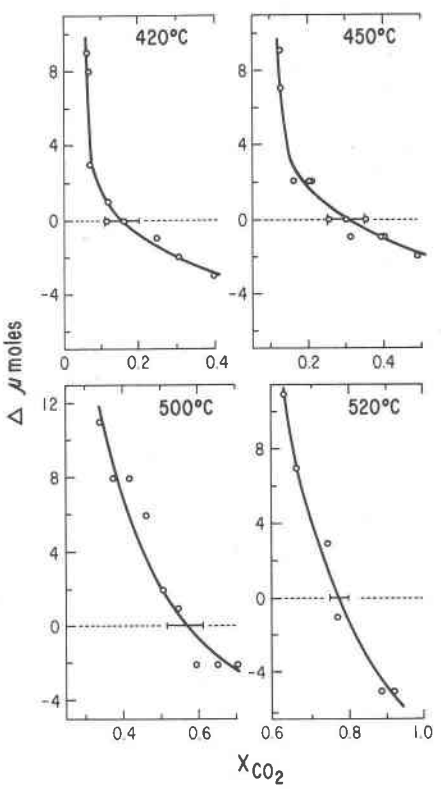

Fig. 4. Experimental data pertaining to equilibrium 4 in H_2O–CO_2 mixtures at P = 2 kbar. Significance of the curves and brackets is identical to those in Figure 1.

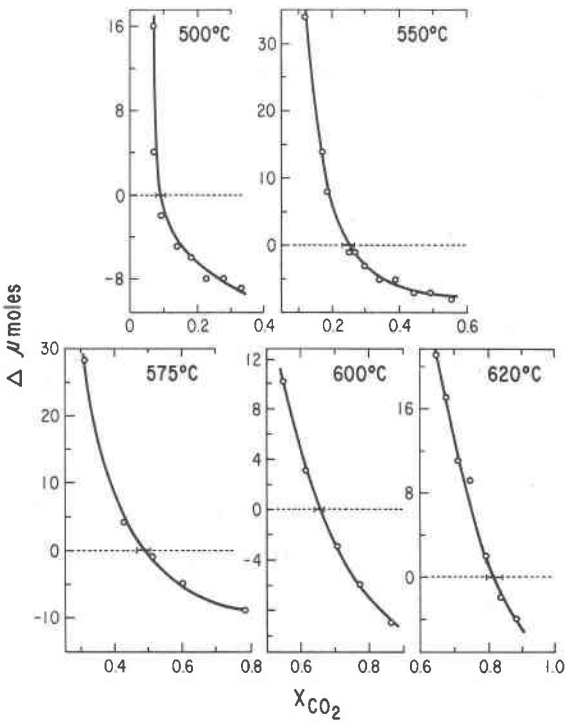

Fig. 5. Experimental data pertaining to equilibrium 4 in H_2O–CO_2 mixtures at P = 6 kbar. Significance of the curves and brackets is identical to those in Figure 1.

X_{CO_2} = 0.58, whereas the upper limit would be the point at X_{CO_2} = 0.65. This method yields an equilibrium X_{CO_2} bracket considerably larger than that determined by the least-squares fit. In essence, the "classical" bracketing method leads to an overestimate of the uncertainty in the X_{CO_2} bracket. Indeed, as demonstrated by Demarest and Hazelton (1981), refined statistical treatment of experimental data may, in many cases, lead to narrower uncertainties in experimentally-determined equilibrium curves. Although data points in the vicinity of the equilibrium crossover can lead to relatively large uncertainties with the "classical" bracketing method, they are very important for constraining the equilibrium location of the fitted curve. Without points close to the crossover there would be considerable latitude in the curvature of the fitted curve and, thus, in the equilibrium X_{CO_2} determination. Further support for the validity of determining equilibrium by the curve-fitting technique is given by the data for the 500°C isotherm in Figure 3. As required theoretically, curves for Δmoles CO_2 and Δmoles quartz, which represent *independent* monitors of reaction, intersect at Δmoles = 0. Hunt and Kerrick (1977), and Eggert and Kerrick (1981) noted similar relationships between independent monitors of reaction rate. Furthermore, except for some slight differences in curvature, the curves for quartz and CO_2 are antithetic (*i.e.*, they are nearly mirror images of one another). This geometric relationship is predicted on the basis that quartz and CO_2 are on the opposite sides of the balanced reaction and that there are equal numbers of moles of these components in the balanced reaction.

The general shape of most of the curves in Figures 1–5 implies that the rate of the forward (CO_2-forming) reaction is faster than the rate of the reverse (CO_2-consuming) reaction. This is evidenced by the fact that the slopes of most curves are steeper for positive values of Δmoles than the curves in the region of negative Δmoles values. This behavior of the slope also implies that the rates of the forward reactions do not reach maximum values, whereas the rates of the reverse reactions do reach maximum values at X_{CO_2} values away from the equilibrium X_{CO_2} value. Hunt and Kerrick (1977) found that a similar relationship existed for the forward and reverse reaction rates of equilibrium 4 as a function of temperature for runs performed at a constant initial X_{CO_2}.

H_2O–CO_2–NaCl fluids

The experimental results on equilibrium 4 in H_2O–CO_2–NaCl fluids are summarized in Figures 6 and 7. The method of determining equilibrium brackets for a particular pressure and temperature is identical to that discussed above for binary H_2O–CO_2 mixtures. The shapes of the curves in Figures 6 and 7 are similar to that of the curves in H_2O–CO_2 mixtures (Figs. 1–5), implying a similar relationship between the forward and reverse reaction rates in NaCl-bearing solutions compared to those in binary H_2O–CO_2 mixtures. The presence of NaCl in the fluid phase may enhance the kinetics of the reactions (compare Figs. 6 and 7 to Figs. 4 and 5), but more data of this type is necessary before any definitive conclusions can be reached regarding the kinetics of the reactions.

Capsules containing only calcite and H_2O–CO_2–NaCl solutions yielded no increase in the mass of CO_2 after a run, implying that there was little or no dissolution of calcite. Optical and X-ray analysis of the run products indicated that no extraneous phases not common to equilibrium 4 formed during the runs. Since equilibrium 4 involves decarbonation, the mass of H_2O before and after a run should remain unchanged, thus providing an additional

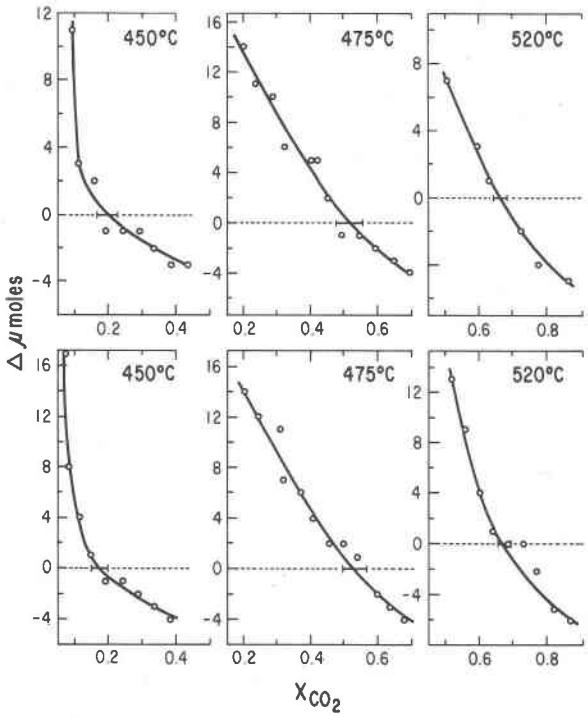

Fig. 6. Experimental data pertaining to equilibrium 4 in H_2O–CO_2–NaCl mixtures at $P = 2$ kbar. Upper set of diagrams: 5 wt. % NaCl; lower set of diagrams: 10 wt. % NaCl. Significance of the curves and brackets is identical to those in Figure 1.

check on any unexpected fluid–solid reactions resulting from the presence of NaCl in the fluid. For all runs, the mass of H_2O remained essentially constant, implying that there were no reactions other than the forward and reverse reactions of equilibrium 4 occurring during the runs.

Some dissolution of Ag from the capsule is expected in Cl-bearing aqueous solutions. For the salinites in our experiments, Seward's (1976) data on the solubility of AgCl in aqueous sodium chloride solutions at 353°C suggests that the concentration of NaCl is ten times larger than that of AgCl. Such low concentrations of AgCl suggest that the activities of components may be quite similar to those in the pure H_2O–CO_2–NaCl system.

Thermodynamic analysis

In this section, experimental equilibrium data are compared to equilibria derived by thermodynamic calculations. From one experimental equilibrium bracket, a curve can be extrapolated in P–T–X_{CO_2} space using available thermodynamic data. The method, discussed in detail by Kerrick and Slaughter (1976), requires evaluating the following equation (equation 17 of Kerrick and Slaughter, 1976) from one experimentally determined starting point (P_1, T_1, K_1) to the P–T–X_{CO_2} conditions of interest (P_2, T_2, K_2):

$$(\Delta G_r)_{T_2}^{P_2} - (\Delta G_r)_{T_1}^{P_1} = 0 = \int_{P_1}^{P_2} \Delta V_r^\circ \, dP - \int_{T_1}^{T_2} \Delta S_r^\circ \, dT + RT_2 \ln K_2 - RT_1 \ln K_1 \qquad (1)$$

The computer programs of Slaughter *et al.* (1976), modified to incorporate HSMRK-derived activity coefficients for H_2O and and CO_2 (Jacobs and Kerrick, 1981), were used for all calculations. Thermodynamic data for pure H_2O and CO_2 were taken from Burnham *et al.* (1969) and Burnham and Wall (unpublished), respectively. High-temperature entropies were calculated from an integrated form of the Maier–Kelley heat capacity equation: $A(\ln T) + B(10^3 \times T) + C(10^5/T^2) + D$. The constants of this equation (A, B, C, and D) for the minerals considered in this study, which are listed in Table 4, were

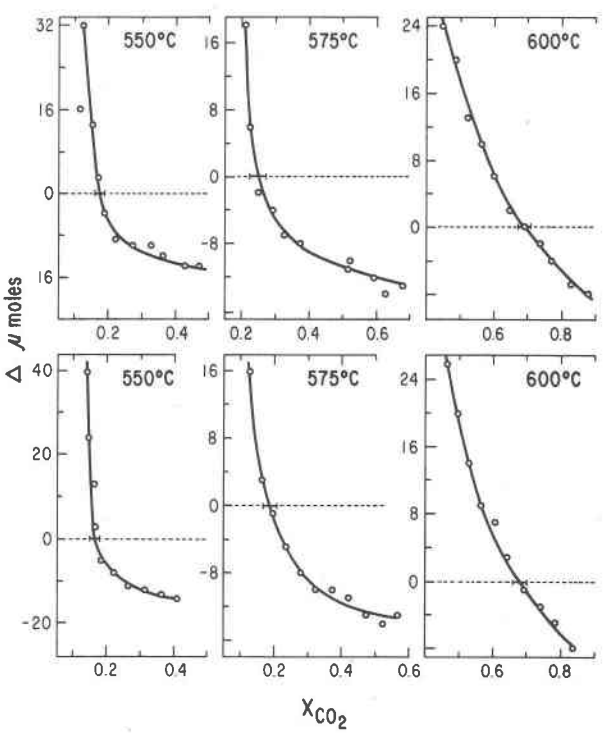

Fig. 7. Experimental data pertaining to equilibrium 4 in H_2O–CO_2–NaCl mixtures at $P = 6$ kbar. Upper set of diagrams: 5 wt. % NaCl; lower set of diagrams: 10 wt. % NaCl. Significance of the curves and brackets is identical to those in Figure 1.

derived from a least-squares fit to the entropy data of Robie and Waldbaum (1968), with the following exceptions: anorthite: Robie *et al.* (1978); diopside: Krupka *et al.* (1980); grossular: Perkins *et al.* (1977); margarite and zoisite: Perkins *et al.* (1980). Extrapolations (both ideal and activity-corrected) were started at experimental equilibrium brackets (P_1, T_1, K_1) which resulted in calculated curves most consistent with the other experimental data.

T–X_{CO_2} relations

Comparison of multiple experimental equilibrium brackets for decarbonation and dehydration equilibria with curves calculated from thermodynamic data gives a direct measure of the activity coefficients for CO_2 and H_2O. Comparisons using "two-volatile" (H_2O–CO_2) equilibria, on the other hand, only give a measure of the ratio or product of activity coefficients for H_2O and CO_2. Nevertheless, both types of equilibria are useful for evaluating the reliability of thermodynamic data and HSMRK-derived activities for H_2O and CO_2. An isobaric T–X_{CO_2} section calculated for equilibrium 2 demonstrates the effect of assuming ideal *versus* non-ideal mixing of H_2O and CO_2 for the calculation of decarbonation equilibria (Fig 8.). At a given pressure and temperature, the difference between the solid and dashed curves is a measure of the activity coefficient for CO_2. As both temperature and pressure are increased, the magnitude of the activity coefficients for CO_2 remains approximately constant, reflecting the offsetting tendencies of increasing pressure and increasing temperature predicted by the HSMRK equation for the P–T increases in Figure 8.

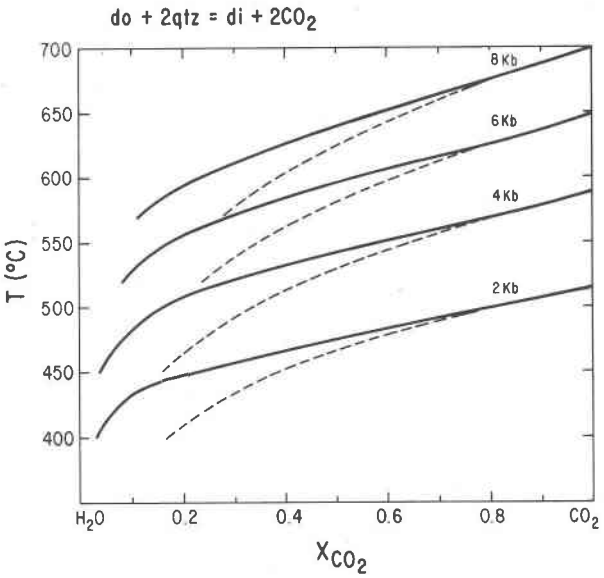

Fig. 8. Calculated isobaric T–X_{CO_2} sections for equilibrium 2. The curves were extrapolated from the experimental bracket at P = 1 kb, T = 442°C, X_{CO_2} = 0.95 of Slaughter *et al.* (1975). The dashed curves were calculated assuming ideal mixing of H_2O and CO_2, whereas the solid curves were calculated using activities for H_2O and CO_2 derived from the HSMRK equation of Kerrick and Jacobs (1981).

Table 4. S_{298} and coefficients for high-temperature entropy equations* of minerals

Phase	S_{298}	A	B	C	D
Andalusite	22.28	42.270	5.516	7.026	-250.260
Anorthite	48.45	68.630	9.397	10.810	-405.700
Calcite	21.92	19.024	13.672	1.442	-114.075
Corundum	12.18	28.792	2.062	5.502	-170.610
Dolomite	37.09	46.830	16.979	8.683	-280.869
Diopside	34.02	55.028	5.865	8.440	-324.625
Forsterite	22.75	35.966	6.688	4.614	-212.128
Gehlenite	47.40	65.262	7.361	9.535	-384.302
Grossular	60.87	105.245	16.022	14.756	-620.978
K-feldspar	56.94	65.573	11.771	9.846	-388.125
Kyanite	20.02	42.874	5.588	7.671	-254.380
Magnesite	15.70	26.314	5.545	6.376	-158.045
Margarite	63.01	94.000	32.741	11.647	-558.379
Muscovite	69.00	98.298	25.440	12.723	-582.200
Periclase	6.44	11.954	0.581	1.696	-70.091
Phlogopite	75.90	105.049	13.693	13.553	-617.675
Quartz	9.88	11.100	8.389	1.331	-67.238
Rutile	12.04	17.633	0.477	2.221	-102.797
Sphene	30.88	45.271	3.395	7.652	-266.587
Talc	62.34	104.487	20.236	19.942	-621.943
Tremolite	131.19	192.908	54.819	26.396	-1144.273
Wollastonite	19.60	27.620	2.854	4.234	-162.650
Zoisite	70.71	98.922	36.357	12.039	-587.914

*Coefficients are for an equation of the form: A (lnT) + B (10^3 x T) + C ($10^5/T^2$) + D.

The experimental equilibrium brackets for equilibria 3 and 4 are shown on log K–$1/T$ diagrams in Figures 9 and 10. Listed in Table 5 are the equations for the straight lines[2], which are plotted on these diagrams and which represent, at any temperature, minimum and maximum values of log X_{CO_2} which are consistent with all of the experimental brackets. This approach is preferred over that of fitting lines of maximum and minimum slope to equilibrium brackets (*e.g.*, Hunt and Kerrick, 1977; Kerrick and Slaughter, 1976; Skippen, 1971), because such lines do not yield realistic uncertainty bands for all P–T–X_{CO_2} conditions of the experiments. For example, in the region where lines of maximum and minimum

[2] Kerrick and Slaughter (1976) demonstrated that there is negligible curvature of mixed-volatile equilibria on log K–$1/T$ diagrams.

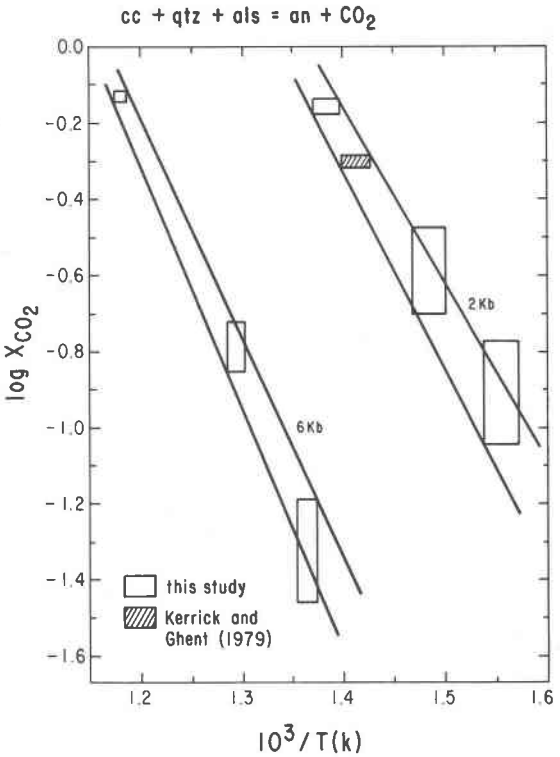

Fig. 9. Log K–1/T diagram showing the experimental brackets of equilibria 3a (2 kbar) and 3k (6 kbar). At each pressure, the two limiting lines outline the error envelope derived by considering uncertainties in all data points. Equations for the lines are listed in Table 5.

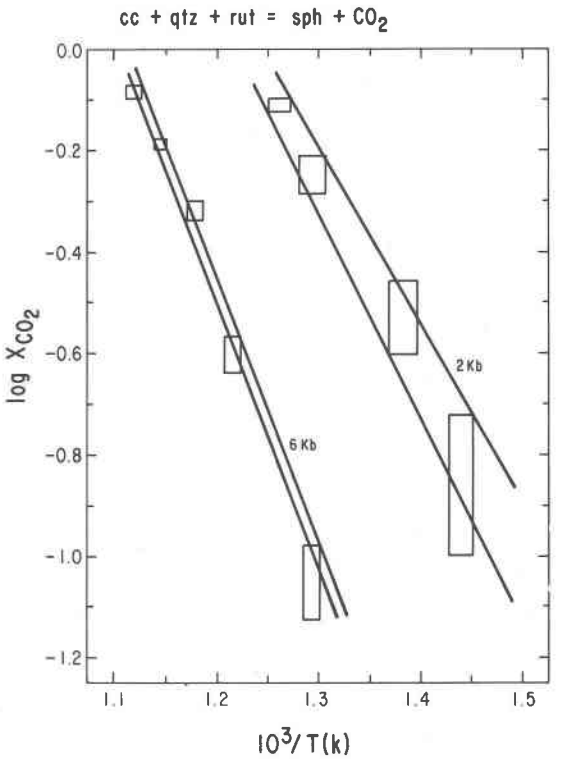

Fig. 10. Log K–1/T diagram showing the experimental brackets of equilibrium 4 at P = 2 and 6 kbar. At each pressure, the two limiting lines outline the error envelope derived by considering uncertainties in all data points. Equations for the lines are listed in Table 5.

slope intersect on log K–1/T diagrams, estimation of an uncertainty band is difficult. In Figures 9 and 10, the series of experimental brackets sufficiently constrain the slope of the lines and the error envelopes of the brackets define the uncertainty band consistent with all the data.

The experimental equilibrium brackets and the uncertainty bands derived from Figures 9 and 10 for equilibria 3 and 4 are plotted together in Figures 11 and 12, respectively. Since the data at each pressure cover a wide range of T–X_{CO_2} values, a stringent test is provided for the thermodynamic data and HSMRK-derived activities for CO_2. The 2 kbar experimental data (see Figures 11 and 12) indicate that ideal mixing of H_2O and CO_2 is an adequate assumption at these P–T conditions. The HSMRK equation predicts only small positive deviations ($\gamma_{CO_2} > 1.0$) from ideality at 2 kbar, which results in calculated curves in good agreement with the experiments except at $T \lesssim 400°$ C (the lower temperature limit investigated by Kerrick and Jacobs, 1981). With the exception of low X_{CO_2} values, curves calculated for equilibrium (3k) at 6 kbar (Fig. 11) assuming ideal mixing and those calculated with HSMRK-derived activities are both in good agreement with the experimental data. However, for equilibrium 4 at 6 kbar (Fig. 12) the curve calculated with HSMRK-derived activities is in much better agreement with the experimental data than that

Table 5. Limiting log K–1/T equations for equilibria 3 and 4*

$$\log X_{CO_2} = a + b\left(\frac{10^3}{T(K)}\right)$$

equilibrium (3a)	P = 2 kb	a = 6.89	5.97
		b = -5.16	-4.38
equilibrium (3k)	P = 6 kb	a = 7.27	6.66
		b = -6.32	-5.71
equilibrium (4)	P = 2 kb	a = 4.82	4.36
		b = -3.97	-3.50
equilibrium (4)	P = 6 kb	a = 5.78	5.84
		b = -5.23	-5.24

* For each equilibrium, the pair of a and b values listed in a column relates to a limiting line plotted in Figures 9 or 10.

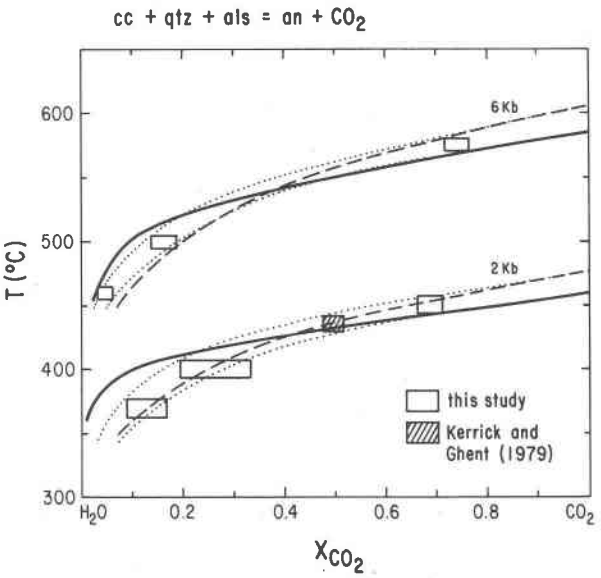

Fig. 11. T–X_{CO_2} sections for equilibria 3a and 3k at $P = 2$ and 6 kbar, respectively. The rectangles are experimental equilibrium brackets. The dotted curves were calculated with the equations in Table 5. The solid and dashed curves were calculated assuming HSMRK-derived activities and ideal mixing of H_2O and CO_2, respectively. The starting points for the ideal and activity-corrected extrapolations were the upper and lower temperature limits at $X_{CO_2} = 1.0$, respectively, calculated with the equations in Table 5.

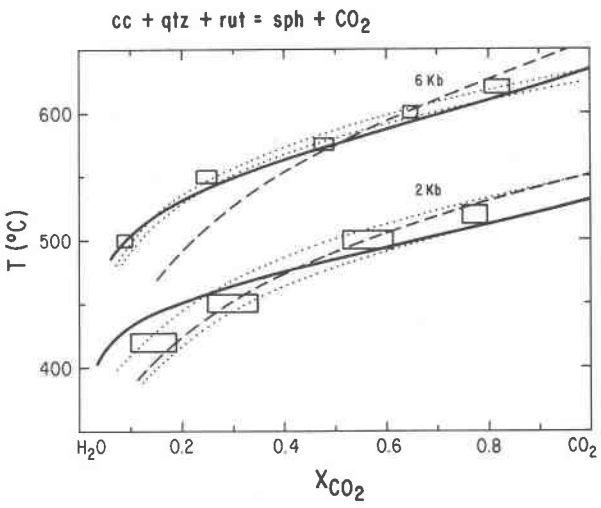

Fig. 12. T–X_{CO_2} sections for equilibrium 4 at $P = 2$ and 6 kbar. The rectangles are the experimental equilibrium brackets. The dotted curves were calculated with the equations in Table 5. The solid and dashed curves were calculated assuming HSMRK-derived activities and ideal mixing of H_2O and CO_2, respectively. The starting points for the ideal and activity-corrected extrapolations at $P = 6$ kbar were $T = 625$°C, $X_{CO_2} = 0.79$ and $T = 615$°C, $X_{CO_2} = 0.85$, respectively. At $P = 2$ kbar, the starting points for the ideal and activity-corrected curves were the upper and lower temperature limits at $X_{CO_2} = 1.0$, respectively, calculated from the equations in Table 5.

calculated with the assumption of ideal mixing of H_2O and CO_2.

A similar T—X_{CO_2} analysis of the HSMRK equation is presented in Figure 13 for the 1 and 2 kbar data of Greenwood (1967) and Harker and Tuttle (1956) on equilibrium 1. At these relatively high temperatures and low pressures, Greenwood (1967) noted that assuming ideal mixing resulted in no significant errors in calculated curves (Fig. 13). At these P–T conditions, the HSMRK equation predicts only slight positive deviations from ideality, resulting in calculated curves in close agreement with the experimentally determined equilibrium data. Equilibrium 1 is again addressed in Figure 14, where data from Ziegenbein and Johannes (1974) and that of the present study are presented. The data in Figure 14 indicate that curves calculated with HSMRK-derived activities result in better agreement with the experiments than those assuming ideal mixing. It should be noted that the 2 kbar data of Greenwood (1967) is inconsistent with that of Ziegenbein and Johannes (1974). However, Greenwood (1967) may have overestimated the experimental temperatures (Kerrick, 1974, p. 741). Overestimation of experimental temperatures may have occurred in the study of Harker and Tuttle (1956) also, since no filler rods were used in the hydrothermal vessels (see Boettcher and Kerrick, 1971). Providing that any errors in temperature measurement in the studies of

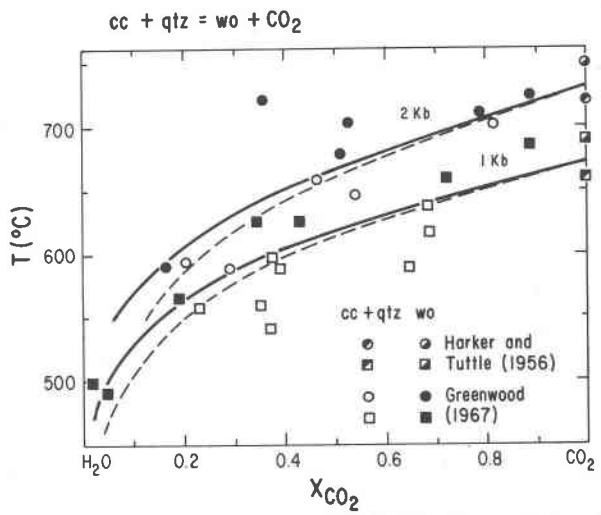

Fig. 13. T–X_{CO_2} sections at $P = 1$ and 2 kbar for equilibrium 1 using the data of Greenwood (1967) and Harker and Tuttle (1956). The solid and dashed curves were calculated assuming HSMRK-derived activities and ideal mixing of H_2O and CO_2, respectively. The starting points for the extrapolations were $P = 1$ kbar, $T = 670$°C, $X_{CO_2} = 1.0$ and $P = 2$ kbar, $T = 730$°C, $X_{CO_2} = 1.0$.

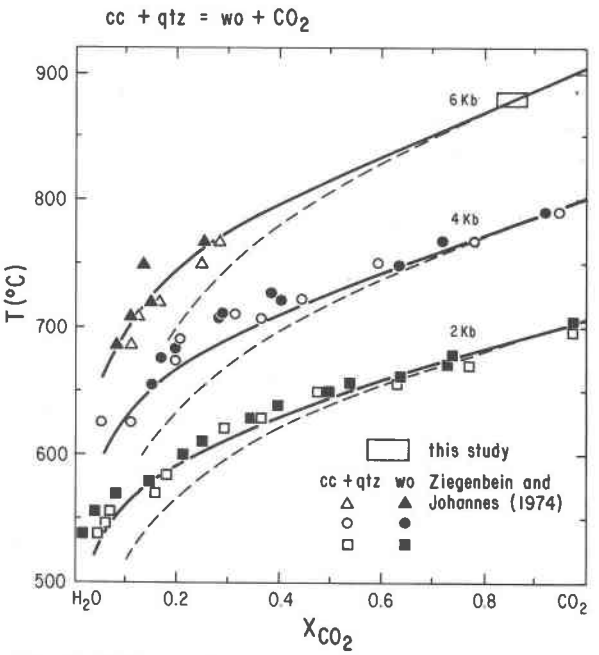

Fig. 14. T–X_{CO_2} sections at P = 2, 4, and 6 kbar for equilibrium 1 using the data from this study and that of Ziegenbein and Johannes (1974). The solid and dashed curves were calculated assuming HSMRK-derived activities and ideal mixing of H_2O and CO_2, respectively.

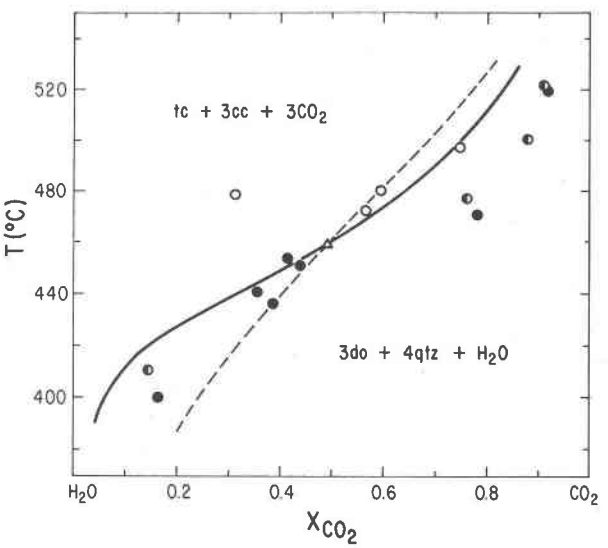

Fig. 15. T–X_{CO_2} section at P = 2 kbar for the equlibrium: 3 dolomite + 4 quartz + H_2O = talc + 3 calcite + 3 CO_2. The experimental data is from Gordon and Greenwood (1970). The filled, half-filled, and open circles represent do + qtz stable, no reaction and tc + cc stable, respectively. The solid and dashed curves were calculated assuming HSMRK-derived activities and ideal mixing of H_2O and CO_2, respectively. The starting point for the extrapolation (triangle) was P = 2 kbar, T = 460°C, X_{CO_2} = 0.50.

Ziegenbein and Johannes (1974) and Greenwood (1967) were systematic and not large, little error should be introduced using this experimental data in the T–X_{CO_2} analysis of this paper.

Figures 15–18 provide a T–X_{CO_2} analysis for mixed-volatile equilibria. In Figure 15 a curve calculated with HSMRK-derived activities provides a much better fit to the experimental data of Gordon and Greenwood (1970) than that calculated assuming ideal mixing (Lewis and Randall rule) of H_2O and CO_2. As shown in Figure 16, similar improvement in calculated curves is obtained for the data of Metz and Puhan (1970, 1971). In addition, from their 6 kbar data on the equilibrium: 5 dolomite + 8 quartz + H_2O = tremolite + 3 calcite + 7 CO_2, Eggert and Kerrick (1981) show that the isobaric T–X_{CO_2} curve calculated with HSMRK-derived activities is in much closer agreement than a curve calculated assuming ideal mixing of H_2O and CO_2. Figure 17 shows that assuming either ideal mixing or HSMRK-derived activities yields calculated curves consistent with the 6 kbar data of Hewitt (1973) on the equilibrium: muscovite + calcite + quartz = K-feldspar + anorthite + H_2O + CO_2. The larger deviation from ideal mixing in the H_2O-rich portion of Figure 17 resulting from calculation

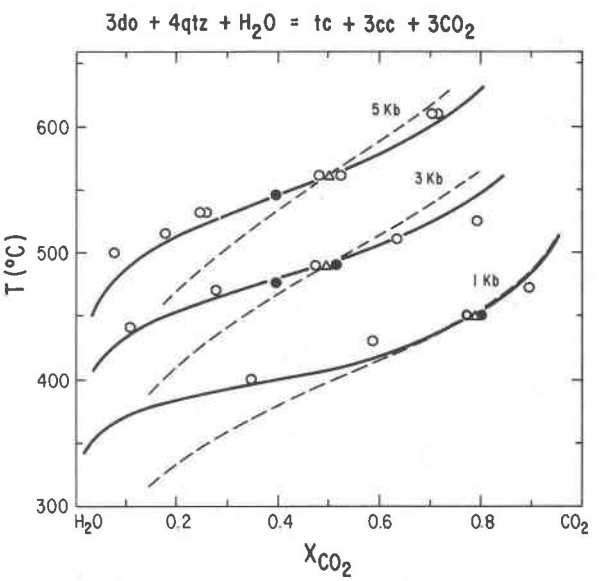

Fig. 16. T–X_{CO_2} sections at P = 1, 3, and 5 kbar for the equilibrium: 3 dolomite + 4 quartz + H_2O = talc + 3 calcite + 3 CO_2. According to Metz and Puhan (1970, 1971), all circles represent equilibrium, with filled circles representing reversal experiments. The starting points for the extrapolations (triangles) are represented by the intersections of the solid and dashed lines, which were calculated assuming HSMRK-derived activities and ideal mixing of H_2O and CO_2, respectively.

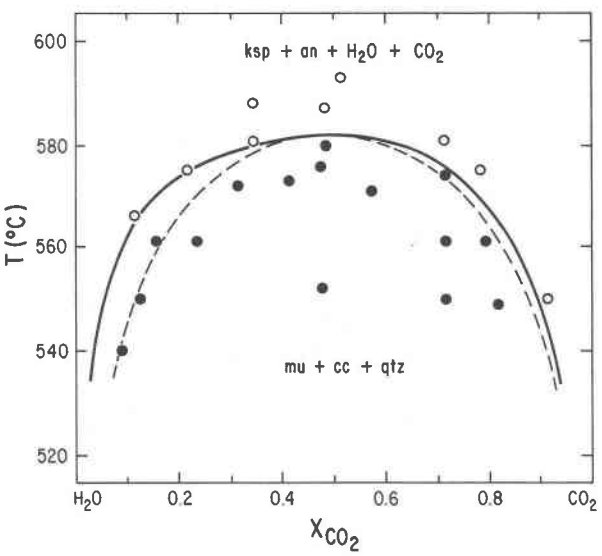

Fig. 17. T–X_{CO_2} section at P = 6 kbar for the equilibrium: muscovite + calcite + 2 quartz = K-feldspar + anorthite + H_2O + CO_2. Experimental data is from Hewitt (1973). The solid circles indicate mu + cc + qtz stable, whereas the open circles indicate ksp + an stable. The solid and dashed curves were calculated assuming HSMRK-derived activities and ideal mixing of H_2O and CO_2, respectively. The starting point for the extrapolations was P = 6 kbar, T = 580°C, X_{CO_2} = 0.5.

with HSMRK-derived activities is compatible with the skewness of the H_2O–CO_2 solvus (Tödheide and Franck, 1963). Figure 18 shows that at both 1 and 5 kbar, HSMRK-derived activities yield calculated curves in better agreement with the data of Metz (1967) on another mixed-volatile equilibrium, though at 1 kbar the difference is not large.

Figures 11–18 illustrate that combining HSMRK-derived activities with thermodynamic data yields calculated curves in close agreement with experimental brackets of many devolatilization equilibria. Figures 19 and 20 illustrate the effect that ideal *versus* non-ideal mixing can have on the calculation of P–T–X_{CO_2} topologies. The magnitude of the effect will depend on the experimental constraints used in the construction of the topology and on the extent of the extrapolations in P–T–X_{CO_2} space. The high (Fig. 19) and low (Fig. 20) temperature portions of the system CaO–Al_2O_3–SiO_2–CO_2–H_2O have been calculated by combining experimental data with thermodynamic extrapolations assuming ideal and non-ideal mixing of H_2O and CO_2. The largest differences in the positions of invariant points occur when extrapolations are made over a wide range of temperature and/or X_{CO_2}. For example, in Figure 19 the stability field of grossular is shifted by approximately 10 mole% to more H_2O-rich compositions at temperatures of 600–800°C when calculated curves are corrected for non-ideal mixing of H_2O and CO_2 with the HSMRK equation. This difference is quite significant for quantifying the P–T–X_{CO_2} conditions of metamorphic assemblages using equilibrium data. As seen in Figure 20, the stability field of zoisite defined by the equilibrium: 2 zoisite + CO_2 = anorthite + calcite + H_2O is significantly expanded at lower temperatures when the calculated curve is corrected for non-ideality in H_2O–CO_2 mixtures via the HSMRK equation. In addition, for the topologies calculated with HSMRK-derived activities, each invariant point in Figure 20 is shifted to higher temperatures (circles) compared to that derived with the assumption of ideal mixing of H_2O and CO_2 (squares).

P–T relations

The T–X_{CO_2} analysis in the preceding section suggests that the thermodynamic data result in calculated curves that are quite consistent with experimental equilibrium data. However, to confidently calculate topologies at a variety of pressures, the consistency of experimental and thermodynamic data as a function of pressure and temperature must be evaluated. As noted in the introduction,

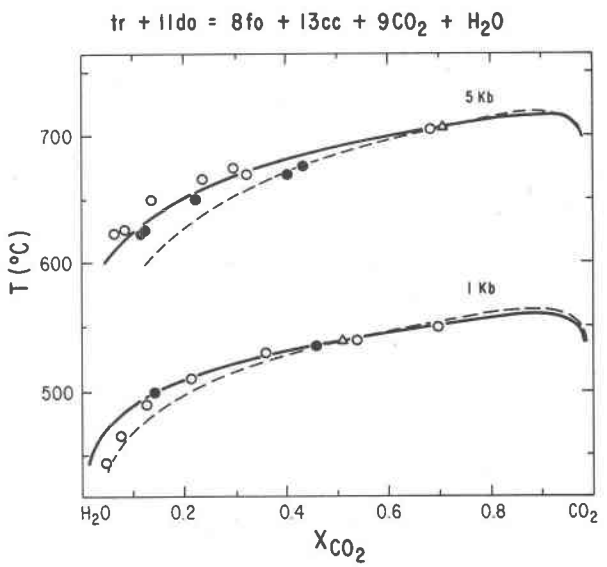

Fig. 18. T–X_{CO_2} sections at P = 1 and 5 kbar for the equilibrium: tremolite + 11 dolomite = 8 forsterite + 13 calcite + 9 CO_2 + H_2O. The experimental data is from Metz (1967, 1976). According to Metz (1967, 1976) the circles represent equilibrium points with filled circles representing reversal experiments. The triangles represent the starting points for the extrapolations.

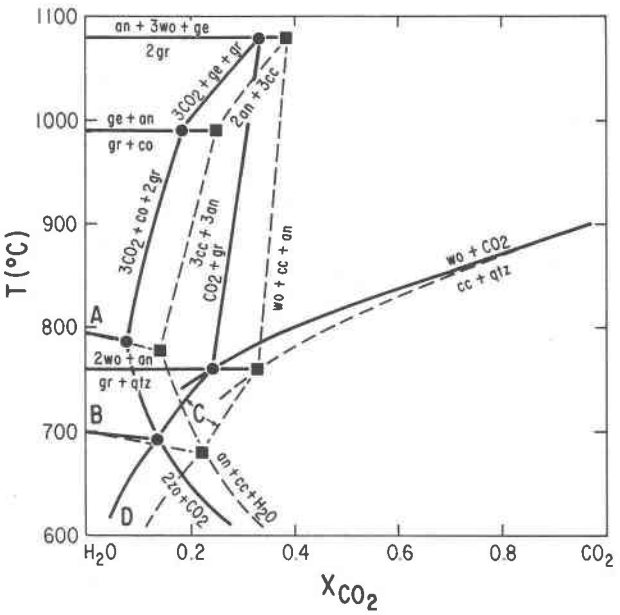

A. $6zo = 6an + 2gr + co + 3H_2O$

B. $4zo + qtz = 5an + gr + 2H_2O$

C. $an + 2cc + qtz = gr + 2CO_2$

D. $2zo + 5cc + 3qtz = 3gr + 5CO_2 + H_2O$

Fig. 19. T–X_{CO_2} section (P = 6 kbar) for a portion of the system CaO–Al_2O_3–SiO_2–H_2O–CO_2. The solid curves and their associated invariant points (circles) were calculated using HSMRK-derived activities for H_2O and CO_2, whereas the dashed curves and their invariant points (squares) were calculated assuming ideal mixing of H_2O and CO_2. In addition to the results of the present experimental study for reaction 1, sources for the experimental data for solid–solid and dehydration equilibria used as starting points (at X_{CO_2} = 0) for the thermodynamic extrapolations are: Boettcher (1970), Huckenholz *et al.* (1975), and Kerrick and Ghent (1979).

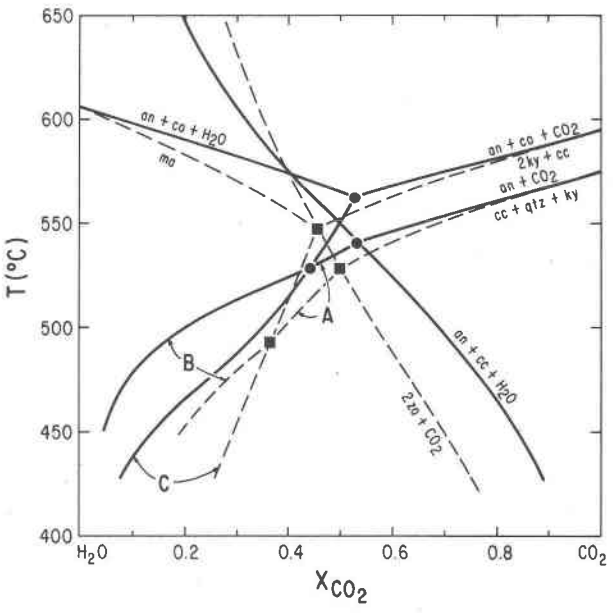

A. $3ky + 4cc + 3qtz + H_2O = 2zo + 4CO_2$

B. $ma + cc + 2qtz = 2an + CO_2 + H_2O$

C. $cc + 2ky + H_2O = ma + CO_2$

Fig. 20. T–X_{CO_2} section (P = 6 kbar) for a portion of the system CaO–Al_2O_3–SiO_2–H_2O–CO_2. Symbols as in Fig. 19. Sources for the equilibria used as starting points for calculating this diagram are: Chatterjee (1974) for the margarite breakdown reaction at X_{CO_2} = 0.0; Kerrick and Ghent (1979) for the two decarbonation equilibria at X_{CO_2} = 1.0.

several authors have carried out such an analysis for solid–solid and dehydration equilibria, but the internal consistency between experiments and thermodynamic calculations for decarbonation and mixed-volatile equilibria has not been thoroughly evaluated. Figures 21–24 provide such an evaluation for several devolatilization equilibria at constant values of X_{CO_2}. In these diagrams, the brackets from this study and that of Eggert and Kerrick (1981) were derived by the statistical curve-fitting method described in the section on Experimental Results, whereas the brackets from other studies are directly from the published paper. In P–T section, little difference exists between curves calculated assuming ideal mixing of H_2O and CO_2 and those calculated using HSMRK-derived activities due to the offsetting effects of pressure and temperature on the activity coefficients for these P–T ranges (see Fig. 8), so for clarity only curves calculated with HSMRK-derived activities are presented in Figures 21-24.

Thermodynamic extrapolations of equilibria 1, 3, and 4 in P–T section are compared to experimental equilibrium brackets in Figure 21. An extrapolation from the 2 kbar data of equilibrium 3 is consistent with the 6 kbar experimental bracket if the total uncertainty in the calculation resulting from errors in the thermodynamic data is considered. The 6 kbar data (at X_{CO_2} = 1.0) for equilibrium 4 lies at temperatures below those derived from an extrapolation from the 2 kbar bracket. However, the equilibrium bracket of Hunt and Kerrick (1977) at 3.5 kbar is in excellent agreement with the extrapolation from 2 kbar. The reason for the discrepancy at 6 kbar for equilibrium 4 is as yet unexplained. As

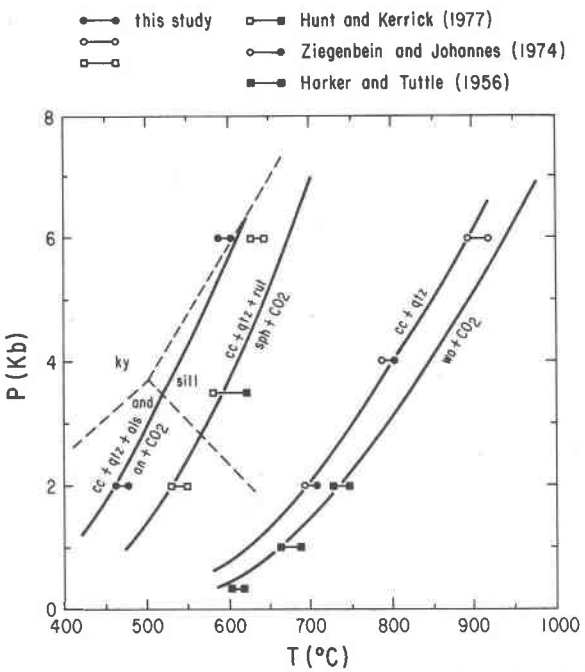

Fig. 21. P–T sections at $X_{CO_2} = 1.0$ for equilibria 1, 3, and 4. The experimental brackets at $X_{CO_2} = 1.0$ were taken from Figs. 11–14. The extrapolations for each equilibrium used the respective 2 kbar brackets as starting points. Note the two extrapolations for equilibrium 1. The Al_2SiO_5 triple point is taken from Holdaway (1971).

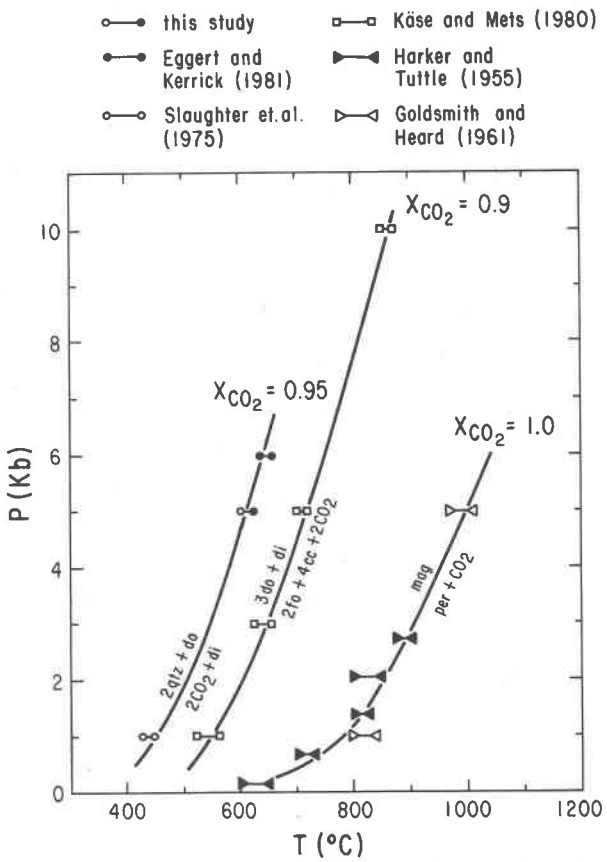

Fig. 22. P–T sections for three decarbonation equilibria. The brackets at $P = 5$ and 6 kbar, $X_{CO_2} = 0.95$ for equilibrium 2, were from the experimental brackets obtained by extrapolation at lower X_{CO_2} values of this study and that of Eggert and Kerrick (1981). The starting points for calculating each P–T curve were the lowest pressure experimental brackets.

seen in Figure 21, comparison of the 6 kbar bracket for equilibrium 1 to the low pressure data of Harker and Tuttle (1956) results in an experimental P–T slope which is too steep relative to that calculated from thermodynamic data. On the other hand, an extrapolation from the 2 kbar bracket of Ziegenbein and Johannes (1974) is in good agreement with the higher pressure data. This analysis supports the earlier suggestion that the experimental temperatures in the study by Greenwood (1967) and Harker and Tuttle (1956) may have been overestimated. As noted before, these inconsistencies associated with equilibria 1 and 4 should in no way alter the conclusions reached from the T–X_{CO_2} analysis of the preceding section, which was accomplished at constant pressure.

Extrapolations for three other decarbonation equilibria, each at a different, constant X_{CO_2} value, are shown in Figure 22. In each case, an extrapolation from the lowest pressure bracket is in excellent agreement with the higher-pressure experimental determinations, implying internal consistency between the thermodynamic data for the various phases involved and the experimental equilibrium brackets.

Figures 23 and 24 illustrate that P–T extrapolations for several mixed-volatile equilibria are also consistent with experimental determinations. Extrapolations of two mixed-volatile equilibria are shown along with experimental determinations in Figure 24. In each case, the agreement between the calculated curve and the experiments is excellent. As seen in Figure 23, calculated P–T slopes for equilibria with H_2O and CO_2 having stoichiometric coefficients of opposite sign are in generally close agreement with experimental determinations. Agreement for an extrapolation from 1 to 6 kbar on the equilibrium in Figure 23B is excellent. The equilibrium extrapolated in Figure 23A is in close agreement with all the experimental equilibrium brackets except the 1 kbar determination of Metz and Puhan (1970, 1971). Considering uncertainties in the entropies for the solid phases alleviates this discrepancy, however. The agreement in Figure

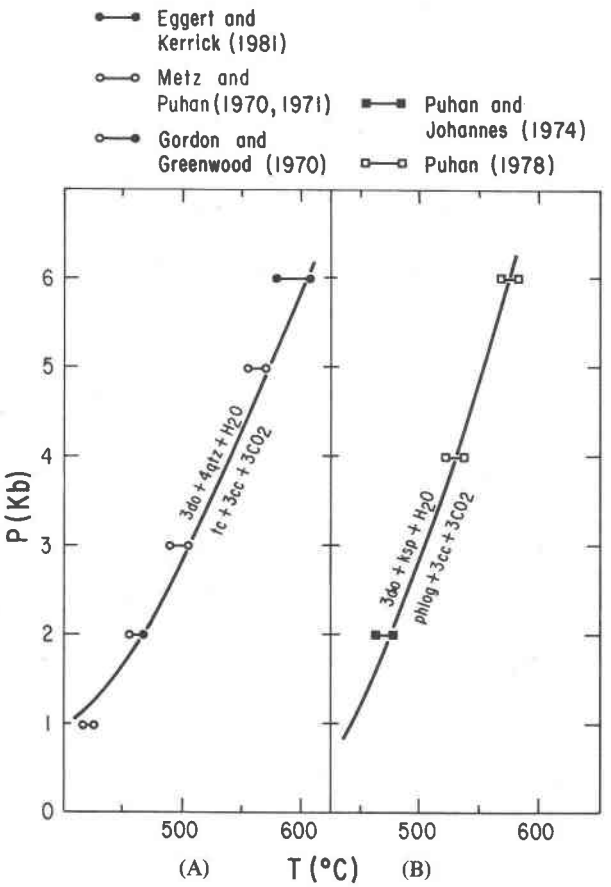

Fig. 23. *P–T* sections at X_{CO_2} = 0.5 for two mixed-volatile equilibria. The starting points for calculating each *P–T* curve were the 2 kbar experimental brackets.

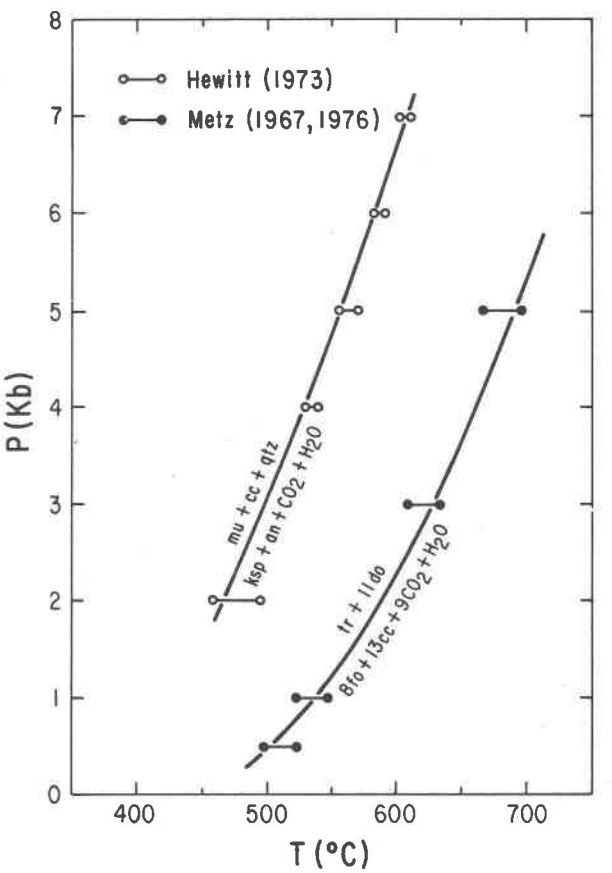

Fig. 24. *P–T* sections at X_{CO_2} = 0.5 for two mixed-volatile equilibria. At all pressures, the brackets were obtained by isobaric extrapolations from the experimental brackets to X_{CO_2} = 0.5. The starting points for calculating each *P–T* curve were within the lowest pressure brackets.

23A is very satisfying, since the experimental data originates from three different hydrothermal laboratories using different methods of determining equilibrium *P–T–*X_{CO_2} conditions.

H_2O–CO_2–NaCl analysis

The importance of precisely quantifying the calculation of *P–T–*X_{CO_2} topologies was illustrated by the analyses in Figures 11–24. However, to best represent geologic systems, the effect which the presence of species in addition to H_2O and CO_2 in the fluid phase has on *P–T–*X_{CO_2} topologies must be considered. Jacobs and Kerrick (1981) have shown that the presence of small amounts of CH_4 can significantly affect the activity relations of H_2O and CO_2, thereby affecting *P–T–*X_{CO_2} topologies. As noted in the introduction, NaCl also has been shown to be an important species in metamorphic fluids.

Figure 25 compares the results of experiments on equilibrium 4 in H_2O–CO_2–NaCl fluids with those in H_2O–CO_2 fluids. At 2 kbar, the experimental equilibrium brackets for both 5 and 10 wt.% NaCl are consistent with the results of experiments in binary H_2O-CO_2 fluids. This agreement implies that, for NaCl salinities of 5–10 wt.% at these *P–T* conditions, the activity of CO_2 is not significantly different from that in binary H_2O–CO_2 fluids. This agreement also suggests that unmixing of the fluid phase does not occur at these *P–T–*X_{CO_2} conditions, although the addition of small amounts of NaCl to H_2O–CO_2 fluids has been shown to expand the solvus (Hendel and Hollister, 1981, Hollister and Burruss, 1976; Takenouchi and Kennedy, 1965). At 6 kbar, little difference is observed between equilibrium brackets in NaCl-bearing *vs.* NaCl-absent fluids at high X_{CO_2} values (Fig. 25). However, for H_2O-rich compositions, significant departures from the equilibrium curve in binary H_2O–CO_2 mixtures are

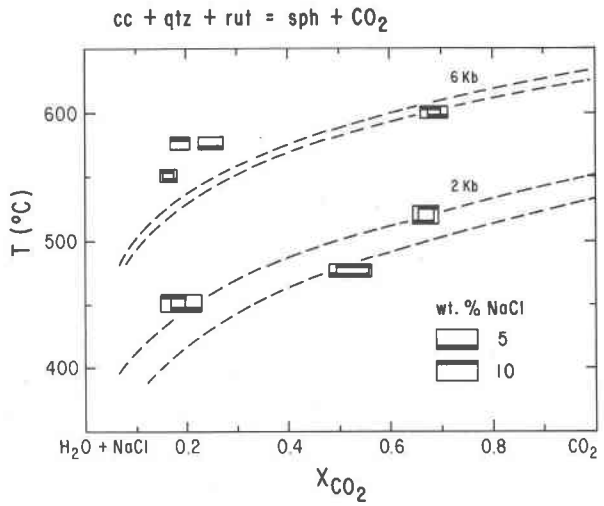

Fig. 25. T–X_{CO_2} sections at P = 2 and 6 kbar for equilibrium 4 in H_2O–CO_2–NaCl mixtures. The wt.% NaCl represents the composition of the aqueous solutions which, along with silver oxalate, were used as starting materials to generate the experimental fluid compositions. The dashed curves were calculated with the equations in Table 5, and represent equilibrium constraints in H_2O–CO_2 mixtures. The rectangles represent experimental determinations of equilibrium 4 in H_2O–CO_2–NaCl mixtures.

observed for both 5 and 10 wt.% NaCl. These departures in H_2O-rich fluids suggest an increased activity of CO_2 resulting from the presence of NaCl in the fluid phase. It has been shown that the addition of NaCl to H_2O–CO_2 fluids expands the solvus (Hendel and Hollister, 1981; Gehrig *et al.*, 1979; Takenouchi and Kennedy, 1965). The experimental data of Gehrig *et al.* (1979) demonstrate that unmixing of the fluid could not have occurred in the runs with 5 wt.% NaCl. Although no experimental data exist for the complete delineation of the solvus for salinities corresponding to our 10 wt.% NaCl runs, extrapolation of the lower salinity data to this composition *suggests* that the solvus in the H_2O–CO_2–NaCl system lies at lower temperatures than those of our experiments. Although more work on this subject is necessary, the implications are clear: the addition of NaCl to H_2O–CO_2 fluids affects the activity of CO_2, thereby affecting the stability of mineral assemblages which are dependent upon the activity of this component.

Discussion

Calculated Clapeyron slopes for decarbonation and mixed-volatile equilibria have been shown to be in good agreement with experimental equilibrium data. As noted in the introduction, several authors have shown similar agreement between calculated and experimental curves for dehydration and solid–solid equilibria. The HSMRK equation of Kerrick and Jacobs (1981) provides reasonable estimates for activities in H_2O–CO_2 mixtures at elevated pressures and temperatures. Consequently, with a few, narrow experimental equilibrium brackets, precise P–T–X_{CO_2} topologies can be calculated for use in the analysis of natural assemblages.

Experimental results on equilibrium 4 in NaCl-bearing fluids reinforce the need to accurately determine the thermodynamic properties of H_2O–CO_2–NaCl solutions over a wide range of pressure and temperature.

Acknowledgments

This study represents part of G. K. Jacobs' Ph.D. research at The Pennsylvania State University. Reviews by I. J. Duncan, D. H. Eggler, T. M. Gordon, P. C. Jurs, A. C. Lasaga, and J. V. Walther on an early draft of this manuscript were very helpful. Discussions with R. G. Eggert, K. M. Krupka, A. C. Lasaga, and R. L. Slingerland were very helpful during the course of the study. We thank J. G. Blencoe, J. Bradbury, R. Erickson, M. Seil, and D. Voight for their assistance in the use of the internally heated pressure vessels. W. Johannes kindly provided the experimental details of the study by Ziegenbein and Johannes (1974). This work was supported in part by grant EAR 76-84199 from the Earth Sciences Division of the National Science Foundation to D. M. Kerrick, and by an Owens–Corning Fiberglas Graduate Fellowship to G. K. Jacobs. The laboratory with the internally heated pressure vessels was maintained by NSF Grant EAR 78-22443 to J. G. Blencoe.

References

Boettcher, A. L. (1970) The system CaO–Al_2O_3–SiO_2-H_2O at high pressures and temperatures. Journal of Petrology, 11, 337–379.

Boettcher, A. L. and Kerrick, D. M. (1971) Temperature calibration in cold-seal vessels. In G. C. Ulmer, Ed., Research Techniques for High Pressure and High Temperature, p. 179–193. Springer-Verlag, New York.

Burnham, C. W., Holloway, J. R., and Davis, N. F. (1969) Thermodynamic properties of water to 1000°C and 10,000 bars. Geological Society of America Special Paper 132, 96 p.

Chatterjee, N. D. (1974) Synthesis and upper stability limit of 2M-margarite, $CaAl_2(Al_2Si_2O_{10}(OH)_2)$. Schweizerische Mineralogische und Petrographische Mitteilungen, 54, 753–767.

Chernosky, J. V. (1979) Experimental metamorphic petrology. Reviews of Geophysics and Space Physics, 17, 860–872.

Chou, I. and Williams, R. J. (1977) Activity of H_2O in CO_2–H_2O at 600°C and pressure to 8 kilobars. Geological Society of America Abstracts with Program, 9, 928.

Chou, I. and Williams, R. J. (1979a) The activity of H_2O in

supercritical fluids: H_2O–CO_2 at 600°C and 700°C at elevated pressures. Tenth Lunar and Planetary Science Conference, 201–203.

Chou, I. and Williams, R. J. (1979b) Activity of H_2O in supercritical CO_2–H_2O fluids. Geological Society of America Abstracts with Program, 11, 401.

Crawford, M. L., Filer, J., and Wood, C. (1979) Saline fluid inclusions associated with retrograde metamorphism. Bulletin de Minéralogie, 102, 562–568.

Crawford, M. L., Kraus, D. W., and Hollister, L. S. (1979) Petrologic and fluid inclusion study of calc-silicate rocks, Prince Rupert, British Columbia. American Journal of Science, 279, 1135–1159.

Daniel C. and Wood, F. S. (1971) Fitting Equations to Data: Computer Analysis of Multifactor Data for Scientists and Engineers, Wiley-Interscience, New York.

Demarest, H. H. Jr. and Haselton, H. T., Jr. (1981) Error analysis for bracketed phase equilibrium data. Geochimica et Cosmochimica Acta, 45, 217–224.

Eggert, R. G. and Kerrick, D. M. (1981) Metamorphic equilibria in the siliceous dolomite system: 6 kb experimental data and geologic implications. Geochimica et Cosmochimica Acta, 45, 1039–1049.

Eggler, D. H. and Burnham, C. W. (1978) Activity of H_2O in diopside and CO_2–H_2O vapor to 20 kilobars, 600–1400°C. Geological Society of America Abstracts with Program, 10, 395.

Eggler, D. H. and Kadik, A. H. (1979) The system $NaAlSi_3O_8$–H_2O–CO_2 to 20 kbar pressure: I. Compositional and thermodynamic relations of liquids and vapors coexisting with albite. American Mineralogist, 64, 1036–1048.

Eggler, D. H., Kushiro, I., and Holloway, J. R. (1979) Free energies of decarbonation reactions at mantle pressures: I. Stability of the assemblage forsterite-enstatite-magnesite in the system MgO–SiO_2–CO_2–H_2O to 60 kbar. American Mineralogist, 64, 288–293.

Flowers, G. C. (1979) Correction to Holloway's (1977) adaptation of the modified Redlich-Kwong equation of state for calculation of the fugacities of molecular species in supercritical fluids of geologic interest. Contributions to Mineralogy and Petrology, 69, 315–318.

Franck, E. U. and Tödheide, K. (1959) Thermische Eigenschaften überkritischer Mischungen von Kohlendioxyd und Wasser bis zu 750°C und 2000 atm.. Zeitschrift für Physikalische Chemie Neue Folge, 22, 232–245.

Gehrig, M., Lentz, H., and Franck, E. U. (1979) Thermodynamic properties of water-carbon dioxide-sodium chloride mixtures at high temperatures and pressures. In K. D. Timmerhaus and M. S. Barber, Eds., High-Pressure Science and Technology, p. 534–542. Plenum Press, New York.

Goldsmith, J. R. and Heard, H. C. (1961) Subsolidus phase relations in the system $CaCO_3$–$MgCO_3$. Journal of Geology, 69, 45–74.

Gordon, T. M. and Greenwood, H. J. (1970) The reaction: dolomite + quartz + water = talc + calcite + carbon dioxide. American Journal of Science, 268, 225–242.

Greenwood, H. J. (1967) Wollastonite: stability in H_2O–CO_2 mixtures and occurrence in a contact-metamorphic aureole near Salmo, British Columbia, Canada. American Mineralogist, 52, 1669–1680.

Greenwood, H. J. (1969) The compressibility of gaseous mixtures of carbon dioxide and water between 0 and 500 bars and 450° and 800° centigrade. American Journal of Science, 267A, 191–208.

Greenwood, H. J. (1973) Thermodynamic properties of gaseous mixtures of H_2O and CO_2 between 450° and 800°C and 0 to 500 bars. American Journal of Science, 273, 561–571.

Harker, R. I. and Tuttle, O. F. (1955) Studies in the system CaO–MgO–CO_2. Part I. The thermal dissociation of calcite, dolomite, and magnesite. American Journal of Science, 253, 209–224.

Harker, R. I. and Tuttle, O. F. (1956) Experimental data on the P_{CO_2}–T curve for the reaction: calcite + quartz = wollastonite + carbon dioxide. American Journal of Science, 254, 239–256.

Helgeson, H. C. (1969) Thermodynamics of hydrothermal systems at elevated temperatures and pressures. American Journal of Science, 267, 729–804.

Helgeson, H. C., Delany, J. M., Nesbitt, H. W., and Bird, D. K. (1978) Summary and critique of the thermodynamic properties of rock-forming minerals. American Journal of Science, 278A, 1–229.

Hendel, E. and Hollister, L. S. (1981) An empirical solvus for CO_2–H_2O–2.6 wt.% salt. Geochimica et Cosmochimica Acta, 45, 225–228.

Hewitt, D. A. (1973) Stability of the assemblage muscovite-calcite-quartz. American Mineralogist, 58, 785–791.

Holdaway, M. J. (1971) Stability of andalusite and the aluminum silicate phase diagram. American Journal of Science, 271, 97–131.

Hollister, L. S. and Burruss, R. C. (1976) Phase equilibria in fluid inclusions from the Khtada Lake metamorphic complex. Geochimica et Cosmochimica Acta, 40, 163–175.

Hollister, L. S., Burruss, R. C., Henry, D. L., and Hendel, E. (1979) Physical conditions during uplift of metamorphic terranes, as recorded by fluid inclusions. Bulletin de Minéralogie, 102, 555–561.

Holloway, J. R. (1977) Fugacity and activity of molecular species in supercritical fluids. In D. G. Fraser, Ed., Thermodynamics in Geology, p. 161–181. D. Reidel Publishing Co., Dordrecht-Holland.

Huckenholz, H. G., Hölzl, E., and Lindhuber, W. (1975) Grossularite, its solidus and liquidus relations in the CaO–Al_2O_3–SiO_2–H_2O system up to 10 kbar. Neues Jahrbuch für Mineralogie Abhandlungen, 12, 000–46.

Hunt, J. A. and Kerrick, D. M. (1977) The stability of sphene: Experimental redetermination and geologic implications. Geochimica et Cosmochimica Acta, 41, 279–288.

Jacobs, G. K. and Kerrick, D. M. (1979) Experimental study of decarbonation equilibria in H_2O–CO_2 mixtures: An evaluation of the mixing properties of H_2O–CO_2 fluids. Geological Society of America Abstracts with Program, 11, 450.

Jacobs, G. K. and Kerrick, D. M. (1980) A simple rapid quench design for cold-seal pressure vessels. American Mineralogist, 65, 1053–1056.

Jacobs, G. K. and Kerrick, D. M. (1981a) Methane: An equation of state with application to the ternary system H_2O–CO_2–CH_4. Geochimica et Cosmochimica Acta, 45, 607–614.

Jacobs, G. K. and Kerrick, D. M. (1981b) APL and FORTRAN programs for a new equation of state for H_2O, CO_2, and their mixtures at supercritical conditions. Computers & Geosciences, 7, 131–143.

Jacobs, G. K., Kerrick, D. M., and Krupka, K. M. (1981) The high temperature heat capacity of natural calcite ($CaCO_3$). Physics and Chemistry of Minerals, 7, 55–59.

Johannes, W. (1969) An experimental investigation of the system MgO–SiO_2–H_2O–CO_2. American Journal of Science, 267, 1083–1104.

Käse, H. and Metz, P. (1980) Experimental investigation of the

metamorphism of siliceous dolomites. IV. Equilibrium data for the reaction: diopside + 3dolomite = 2forsterite + 4calcite + 2 CO_2. Contributions to Mineralogy and Petrology, 73, 151–159.

Kerrick, D. M. (1974) Review of metamorphic mixed-volatile (H_2O–CO_2) equilibria. American Mineralogist, 59, 729–762.

Kerrick, D. M. and Ghent, E. D. (1979) P–T–X_{CO_2} relations of equilibria in the system CaO–Al_2O_3–SiO_2–CO_2–H_2O. In V. A. Zharikov, V. I. Fonarev, and S. P. Korikovskii, Eds., Problems of Physicochemical Petrology, D. S. Korzhinskii Commemorative Volume 2, p. 32–52.

Kerrick, D. M. and Jacobs, G. K. (1981) A modified Redlich-Kwong equation for H_2O, CO_2, and H_2O–CO_2 mixtures at elevated pressures and temperatures. American Journal of Science, 281, 735–767.

Kerrick, D. M. and Slaughter, J. (1976) Comparison of methods for calculating and extrapolating equilibria in P–T–X_{CO_2} space. American Journal of Science, 276, 883–916.

Konnerup-Madsen, J., Larsen, E., and Rose-Hansen, J. (1979) Hydrocarbon-rich fluid inclusions in minerals from the alkaline Ilimaussag intrusion, South Greenland. Bulletin de Minéralogie, 102, 642–653.

Krupka, K. M., Kerrick, D. M., and Robie, R. A. (1980) Heat capacities from 5 to 1000 K for natural diopside, wollastonite, and orthoenstatite (abstr.) Trans. American Geophysical Union, 61, 407.

Luckscheiter, A. B. and Morteani, G. (1980) Microthermometrical and chemical studies of fluid inclusions in minerals from Alpine veins from the penninic rocks of the central and western Tauern Window (Austria/Italy). Lithos, 13, 61–77.

Metz, P. (1967) Experimentelle Bildung von Forsterit und Calcit aus Tremolit und Dolomit. Geochimica et Cosmochimica Acta, 31, 1517–1532.

Metz, P. (1976) Experimental investigation of the metamorphism of siliceous dolomites III. Equilibrium data for the reaction: tremolite + lldolomite = 8forsterite +13calcite + 9CO_2 + H_2O. Contributions to Mineralogy and Petrology, 58, 137–148.

Metz, P. and Puhan, D. (1970) Experimentelle Untersuchung der Metamorphose von kieselig dolomitischen Sedimenten I. Die Gleichgewichtsdaten der reaktion 3 dolomit + 4quartz + H_2O = talc + 3calcit + 3CO_2 fur die Gesamtgasdrucke von 1000, 3000, und 5000 bar. Contributions to Mineralogy and Petrology, 26, 302–314.

Metz, P. and Puhan, D. (1971) Korrektur zur Arbeit "Experimentelle Untersuchung der Metamorphose von kieselig dolomitischen Sedimenten I. Die Gleichgewichtsdaten der reaktion 3dolomit + 4quarz + H_2O = talc + 3calcit + 3CO_2 fur die Gesamtgasdrucke von 1000, 3000, und 5000 bar." Contributions to Mineralogy and Petrology, 31, 169–170.

Newton, R. C. (1965) The thermal stability of zoisite. Journal of Geology, 73, 431–441.

Pêcher, A. (1979), Les inclusions fluides des quartz d'exsudation de la zone du M. C. T. himalyen au Népal central: données sur la phase fluide dans une grande zone de cisaillment crustal. Bulletin de Minéralogie, 102, 537–554.

Perkins, D. P. III, Essene, E. J., and Westrum, E. F., Jr. (1977) Application of new thermodynamic data to grossular phase relations. Contributions to Mineralogy and Petrology, 64, 137–147.

Perkins, D. P. III, Westrum, E. F., Jr., and Essene, E. J. (1980) The thermodynamic properties and phase relations of some minerals in the system CaO–Al_2O_3–SiO_2–CO_2–H_2O. Geochimica et Cosmochimica Acta, 44, 61–84.

Puhan, D. (1978) Experimental study of the reaction: dolomite + K-feldspar + H_2O = phlogopite + calcite + CO_2 at the total gas pressures of 4000 and 6000 bars. Neues Jahrbuch für Mineralogie Monatshefte, 3, 110–127.

Puhan, D. and Johannes, W. (1974) Experimentelle Untersuchung der reaktion Dolomit + Kalifelspat + H_2O = Phlogopite + Calcit + CO_2. Contributions to Mineralogy and Petrology, 48, 23–31.

Rich, R. A. (1979) Fluid inclusion evidence of Silurian evaporites in southeastern Vermont. Geological Society of America Bulletin, 90, Pt. II, 1628–1643.

Robie, R. A. and Waldbaum, D. R. (1968) Thermodynamic properties of minerals and related substances at 298.15 K (25°C) and 1 atmosphere (1.013 bars) pressure and higher temperatures. U.S. Geological Survey Bulletin 1259.

Robie, R. A., Hemingway, B. S., and Fisher, J. R. (1978) Thermodynamic properties of minerals and related substances at 298.15K and 1 bar (10^5 Pascals) pressure and at higher temperatures. U. S. Geological Survey Bulletin 1452.

Roedder, E. (1972) The composition of fluid inclusions. In M. Fleischer, ed., Data of Geochemistry, p. 000–000. U. S. Geological Survey Professional Paper 440 JJ.

Ryan, T. A., Jr., Joiner, B. L., and Ryan, B. F. (1976) Minitab Student Handbook. Duxbury Press, Scituate, Massachusetts.

Seward, T. M. (1976) The stability of chloride complexes of silver in hydrothermal solutions up to 350°C. Geochimica et Cosmochimica Acta, 40, 1329–1341.

Shmulovich, K. I. (1977) Stability limits of grossular and wollastonite in the H_2O–CO_2 system up to 6 kbar. Geokhimiya, 12, 1806–1816, (transl., Geochemistry International, 14, 126–134.

Shmulovich, K. I. and Shmonov, V. M. (1978) Tables of thermodynamic Properties of Gases and Liquids (Carbon Dioxide). Gosdarstvennaya Sluzhba Standartnykh Spravochnykh Dannykh.

Skippen, G. B. (1971) Experimental data for reactions in siliceous marbles. Journal of Geology, 79, 457–481.

Slaughter, J., Kerrick, D. M., and Wall, V. J. (1975) Experimental and thermodynamic study of equilibria in the system CaO–MgO–SiO_2–CO_2–H_2O. American Journal of Science, 275, 143–162.

Slaughter, J., Wall, V. J., and Kerrick, D. M. (1976) APL computer programs for thermodynamic calculations of equilibria in P–T–X_{CO_2} space. Contributions to Mineralogy and Petrology, 54, 157–171.

Takenouchi, S. and Kennedy, G. C. (1965) The solubility of carbon dioxide in NaCl solutions at high temperatures and pressures. American Journal of Science, 263, 445–454.

Tödheide, K. and Franck, E. U. (1963) Das Zweiphasengebiet und die kritische Kurve im System Kohlendioxyd-Wasser bis zu Drucken von 3500 bar. Zeitschrift für Physikalische Chemie Folge, 37, 387–401.

Wall, V. J. and Essene, E. J. (1972) Subsolidus equilibria in CaO–Al_2O_3–SiO_2–H_2O. (abstr.) Geological Society of America Abstracts with Program, 4, 700.

Walter, L. S. (1963) Data on the fugacity of CO_2 in mixtures of CO_2 and H_2O. American Journal of Science, 261, 151–156.

Ziegenbein, P. and Johannes, W. (1974) Wollastonitbildung aus Quarz und Calcit bei P_f = 2, 4, und 6 kb. Fortschritte der Mineralogie, 52, 77–79.

Ziegenbein, P. and Johannes, W. (1980) CO_2 Aktivitäten in überkritischen CO_2–H_2O Mischungen: Experimentell bestimmte Abweichung von der idealen Mischbarkeit. Fortschritte der Mineralogie, 58, 142–144.

Manuscript received, November 10, 1980;
accepted for publication, June 26, 1981.